Control of photoswitching kinetics with strong light-matter coupling in a cavity

Hongfei Zeng,[1] Pufan Liu,[1] Christopher T. Eckdahl,[2] Juan B. Pérez-Sánchez,[3] Woo Je Chang,[2,4] Emily A. Weiss,[2,4] Julia A. Kalow,*[2] Joel Yuen-Zhou,*[3] Nathaniel P. Stern*[1]

[1]Department of Physics and Astronomy, Northwestern University, Evanston, IL 60208, United States

[2]Department of Chemistry, Northwestern University, Evanston, IL 60208, United States

[3]Department of Chemistry and Biochemistry, University of California–San Diego, La Jolla, CA 92093, United States

[4]Department of Materials Science and Engineering, Northwestern University, Evanston, IL 60208, United States

ABSTRACT: Most photochemistry occurs in the regime of weak light-matter coupling, in which a molecule absorbs a photon and then performs photochemistry from its excited state. In the strong coupling regime, enhanced light-matter interactions between an optical field and multiple molecules lead to collective hybrid light-matter states called polaritons. This strong coupling leads to fundamental changes in the nature of the excited states including multi-molecule delocalized excitations, modified potential energy surfaces, and dramatically altered energy levels relative to non-coupled molecules. The effect of strong light-matter coupling on covalent photochemistry has not been well explored. Photoswitches undergo reversible intramolecular photoreactions that can be readily monitored spectroscopically. In this work, we study the effect of strong-light matter coupling on the kinetics of photoswitching within optical cavities. Reproducing prior experiments, strong coupling causes decelerated photoswitching in spiropyran/merocyanine photoswitches. Fulgide photoswitches, however, show the opposite effect, with strong coupling accelerating photoswitching. While modified merocyanine switching can be explained by changes in radiative decay rates, modifications of fulgide switching kinetics suggest direct changes to excited-state reaction kinetics.

INTRODUCTION

Traditional photochemistry involves the interaction between a single absorber and a single photon. A molecule or complex absorbs a photon and is promoted to an electronically excited state from which it can perform various energy conversion processes and ultimately react intra- or intermolecularly. This model fails in the strong coupling regime in which the rate of energy exchange between light and matter is faster than dissipation processes. This regime is accessible when a photon mode interacts coherently with an ensemble of molecules so that the molecular excitation and cavity photon eigenmodes are replaced by new hybrid states that have both photonic and molecular excitonic characteristics. The new eigenmodes of the system are called the upper (UP) and lower polariton (LP), which correspond to the two branches of eigenenergies, respectively (**Figure 1a**).[1] The energy difference between the upper and lower polariton at resonance, which is referred to as the vacuum Rabi splitting, is given by Eq 1:

$$\hbar\Omega_R = 2\sqrt{N}\hbar g_s \quad (1)$$

where $\hbar g_s$ is the single particle light-molecule coupling strength, and N is the number of molecules in the ensemble. In addition to the polaritonic states, N-1 "dark" states emerge.[1]

Strong coupling between light and molecular excitations has emerged as a strategy to influence chemical reactivity. One common way to achieve strong coupling is to embed chromophores into a cavity that is resonant with the chromophore's transition (**Figure 1a**).[2] Coupling of vibrational excitations to infrared cavities has led to dramatic changes in thermal reaction rates.[3–5] The influence of optical polaritons on photochemical processes has received comparatively less attention. Although some works show negligible changes in photophysics due to strong coupling,[6,7] other studies of optical cavities have demonstrated polaritonic effects on spin or energy conversion processes such as intersystem crossing, triplet-triplet annihilation, and resonant energy transfer.[8–16]

Only two experimental studies have investigated polaritonic effects on covalent photochemical reactions.[17,18] Photoswitches represent ideal systems in which to study polaritonic effects on photochemistry, since the isomerization of photoswitches is unimolecular, reversible, and easily monitored by spectral changes. Moreover, if only one isomer is able to couple to the cavity mode, a photoswitch-cavity system can be reversibly moved in and out of the strong coupling regime thanks to the dependence of Rabi splitting on the number of coupling molecules (**Figure 1b**).[19] In their seminal 2012 study, Hutchison *et al.* reported that the kinetics of the isomerization of a spiropyran (SPI)/merocyanine (MC) photoswitch was modified by coupling of the MC isomer to an optical cavity mode (**Figure 1c**).[17] Strong coupling to the cavity decreased the overall rate of attainment of photostationary state (PSS) and led to a PSS within the cavity containing a higher proportion of MC than the corresponding PSS outside of the cavity. The authors attributed both of these effects to

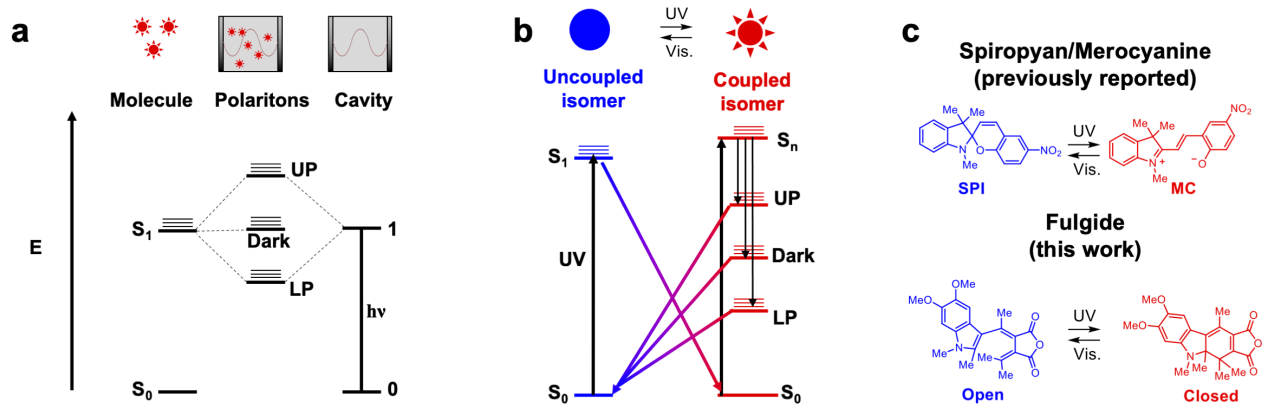

Figure 1. **(a)** Energy level diagram of the light-matter coupling process between an optical cavity mode and resonant molecules. Collective strong coupling leads to the emergence of two polaritonic states, upper (UP) and lower polariton (LP), and uncoupled dark states. **(b)** Illustration of photoswitching in an optical cavity. One isomer is uncoupled, and the visible-light absorbing isomer is capable of strong coupling. Photoswitching could then plausibly occur from either polaritonic state or the dark states. **(c)** The molecular structures and photoisomerization reaction of spiropyran (SPI)/merocyanine (MC) and fulgide molecules.

the change in energy levels introduced by strong coupling: the lower energy of the lower polariton relative to the non-coupled excited molecule led it to relax back to the ground state through cavity leakage, which thereby decreased the photoisomerization efficiency and increased the PSS MC concentration. A more recent report by Börjesson and coworkers studied the effect of strong coupling on the photoisomerization of a norbornadiene-quadricylane photoswitch system.[18] The authors did not study photoisomerization kinetics, but instead measured the quantum yield of the coupled and non-coupled system. They found that the quantum yield of photoisomerization upon excitation of the lower polariton state is significantly lower than that of the bare molecular exciton or of the upper polariton. The authors explained this effect as arising from a competition between cavity leakage and energetically unfavorable conversion to dark states following lower polariton excitation. Unlike in Hutchison's study, Börjesson *et al.* observed no change to photoswitching behavior when exciting to higher energy states than the lower polariton. In summary, previous studies of polaritonic effects on photoswitching have observed a suppression of photoswitching under strong light-matter coupling conditions.

We herein expand experimental investigations of polaritonic photochemistry to a fulgide photoswitch (**Figure 1c**). Unlike the previously reported photoswitches discussed above, fulgides are P-type, meaning they do not engage in any thermal isomerization. Moreover, they switch between their open and closed states via a 6π electrocylization/reversion mechanism, similar to diarylethenes, which is distinct from the previously reported photoswitches.[20] We additionally recapitulate Hutchison's original SPI/MC results in order to confidently compare the two photoswitches. We find that the two molecules exhibit different polaritonic effects: while the MC-to-SPI photoisomerization efficiency is decreased due to enhanced radiative relaxation, the analogous closed-to-open isomerization of the fulgide is enhanced in the strong coupling regime. We explain this effect as arising from an increase in the rate of fulgide ring opening under strong-light matter coupling conditions.

RESULTS AND DISCUSSION

To maximize the change in concentration before and after irradiation (i.e. high PSS) and thus access larger Rabi splitting, we synthesized an all-visible-switching indolyl fulgide that has two isomers, open and closed (see Supporting Information (SI) for synthetic details and molecular spectra).[21] The fulgide molecules were dispersed in a polymethyl methacrylate (PMMA) matrix and put inside a Fabry-Pérot cavity that consists of two parallel silver mirrors deposited by thermal evaporation (**Figure 2a**). Two additional polyvinyl alcohol (PVA) layers were spin-coated to encapsulate the PMMA matrix and isolate the molecules from direct metal deposition and to avoid a plasmonic effect of silver.[2,22] A portion of the sample was masked during the top silver deposition, creating a region without the top silver mirror to directly measure the molecules outside a cavity, referred to as the off-cavity region. The region with top silver is referred to as the on-cavity region and the cavity mode is tuned to be resonant with the closed isomer absorption around λ_{max} = 670 nm by controlling the layer thicknesses.

The fulgide cavity exhibited fully switchable strong coupling. The reflectance spectrum shows a sharp cavity mode following switching to the non-coupled, open state of the fulgide via red light irradiation (**Figure 2c**). Irradiation with blue light switched the fulgide to the closed state whose absorption is near resonant to the cavity mode. The closed isomer does not absorb blue light, leading to its accumulation. With long enough irradiation time, sufficient open isomers are converted to the closed form, and the cavity reaches strong coupling, as evidenced by the emergence of upper and lower polariton peaks in the reflectance spectrum. Measurement of the reflectance spectrum in the off-cavity region revealed a non-split molecular absorbance and can also indicate the concentration of closed form (**Figure 2b**). The fulgide photoswitches bidirectionally; therefore the coupling strength can be tuned reversibly between no coupling and strong coupling.

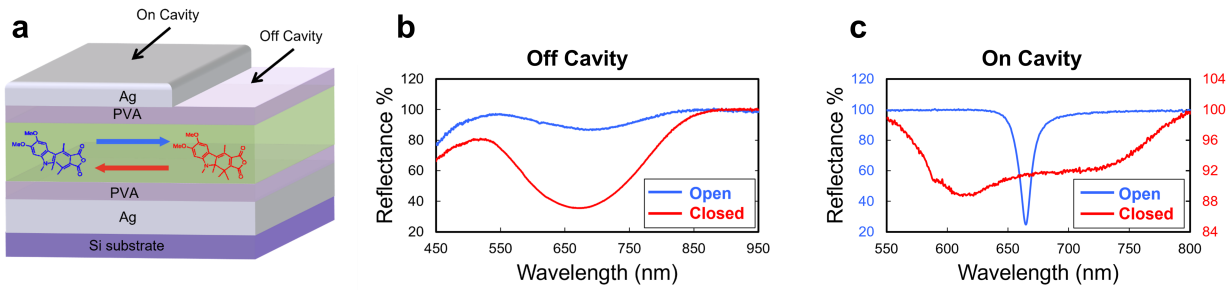

Figure 2. (**a**) Schematic of the cavity samples used in this work. The photoswitch molecules in a PMMA polymer matrix are encapsulated by PVA buffer layers and two parallel silver mirrors. On-cavity measurements are made where both mirrors are present, while off-cavity measurements are made where there is no top mirror. (**b**) Reflectance spectrum of the off-cavity region shows a single broad, switchable feature from the photoswitch (blue/red when molecules are mostly in the open/closed form, respectively). (**c**) Reflectance spectrum of the on-cavity region shows a sharp cavity mode (blue) when the photoswitch is in the uncoupled isomer, but switching to the coupled isomer leads to two distinct polaritonic peaks (red), indicative of strong coupling.

After fabricating and establishing the photoswitchability of the fulgide-containing cavity, we next measured and analyze the photoswitching kinetics. We began in the strong coupling regime with a maximized population of closed isomer, and irradiated the system with UV light at 325 nm. The use of UV irradiation simplifies the experiment because 1) silver has a transparency window near 325 nm, and 2) both isomers have similar absorption coefficients at 325 nm, regardless of coupling strength (**Figure S6**). Taken together, these two features of 325 nm irradiation mean that the amount of photons absorbed by the system does not depend on the coupling strength or distribution of isomers during the photoswitching experiment. Note that the visible light-absorbing closed fulgide will be excited into high lying excited states, S_n, by the UV light before quickly relaxing to the first excited state, S_1, or a polaritonic state, as depicted in **Figure 1b**.

We measured the reflectance spectra as a function of UV irradiation time as the closed isomers converted to the open form and eventually reached the PSS (**Figure 3a-c**). We modeled the reflectance using the transfer matrix method with the polymer matrix including molecules treated as a layer in the cavity characterized by a Lorentz oscillator model of the refractive index. The strongly coupled isomer concentration, which is proportional to the oscillator strength in the model, was extracted by fitting the reflectance spectrum at each irradiation time to the model, allowing for kinetics analysis. For a steady-state reaction with rate constant k, the product or starting material concentration be written in a linear form by defining a quantity $q(t)$ as

$$q(t) \equiv \ln \frac{[\mathrm{A}](t)-[\mathrm{A}](\infty)}{[\mathrm{A}](0)-[\mathrm{A}](\infty)} = -kt \qquad (2)$$

In Eq 2, $[\mathrm{A}](t)$ is the concentration of the species of interest at time t and $[\mathrm{A}](\infty)$ is the concentration at the end of the experiment. The photoisomerization kinetics from closed isomers to open isomers upon UV irradiation is analyzed and plotted in **Figure 3d** and **3e.** Although we targeted the silver transparency window, the intensity of UV was different in the on cavity and off cavity regions, and we corrected this difference by fabricating and measuring an off-resonance cavity sample with thicker PMMA and PVA layer thicknesses with a cavity mode at 830 nm, spectrally distinct from any molecule absorption. As shown in **Figure 3d**, both on- and off-cavity kinetics in the off-resonance cavity show a linear trend and are well aligned after the light intensity correction, which is expected in the absence of strong coupling. In the on-resonance sample, while the off-cavity result is still linear, the on-cavity result is clearly non-linear (**Figure 3e**). At the beginning of the experiment, in the strong coupling regime, the magnitude of the slope is greater, but then gradually levels off to be parallel to the off-cavity data as the coupling strength decreases. Comparison to the non-resonant cavity indicates that the different behavior in the resonant cavity can be attributed entirely to strong coupling. The increase in the magnitude of the slope at early times, when the concentration of closed form is high, indicates that strong coupling acts to increase the rate of the closed-to-open photoswitching reaction. That is, in the fulgide cavity, strong coupling increases the rate of the photoreaction that depletes the strongly coupled isomer.

Similar measurements had been conducted with SPI/MC by Hutchison *et al.* previously.[17] In the SPI/MC system, the cavity acts to increase the concentration of MC at the 325 nm PSS. Further, the SPI/MC system approaches the PSS more slowly once it enters the strong coupling regime. According to Hutchison, these changes originate from an enhancement of the MC radiative decay rate in the strong coupling regime, which manifests as an overall decrease in photoswitching kinetics. In order to validate our comparison between fulgide and SPI/MC cavity modification, we recapitulated Hutchison's observations and data analysis (**Figure S11**). In summary, strong coupling increases the rate at which the fulgide cavity approaches the PSS, while it decreases the rate that the SPI/MC cavity does so.

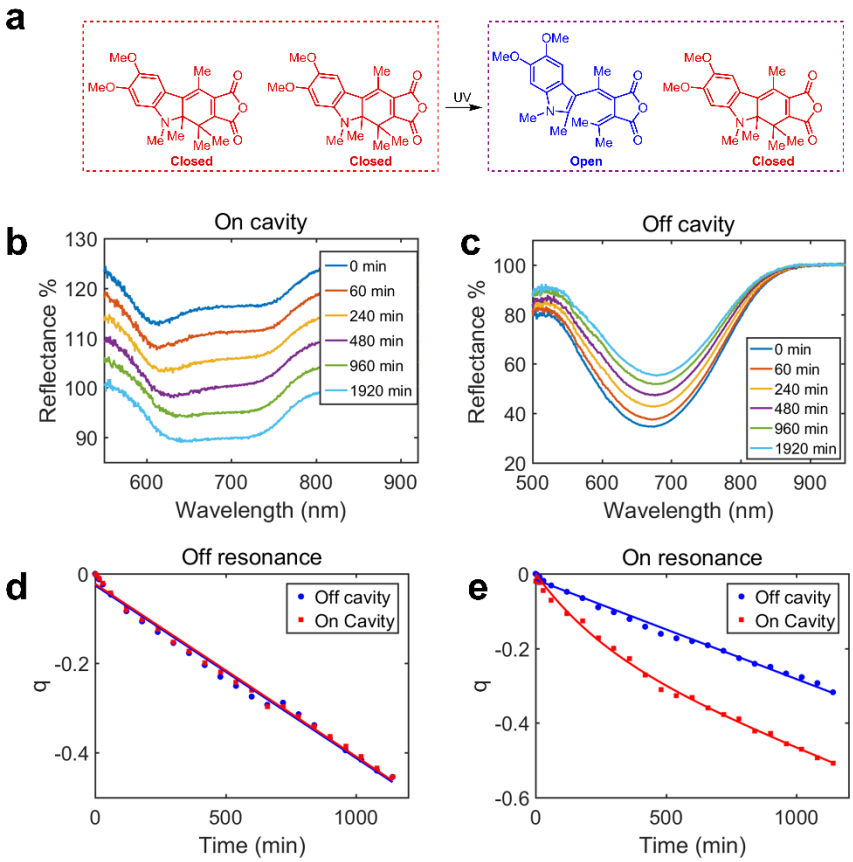

Figure 3. **(a)** Illustration of the photoswitching reaction upon UV irradiation, starting from a full population of closed isomers to a mixture of closed and open isomers. **(b)** Reflection spectra of the on-cavity region as a function of UV irradiation time. The spectra are shifted in y-axis for better visualization. UV irradiation gradually brings the system out of strong coupling, as evidenced by the disappearance of Rabi splitting in the reflectance spectrum. **(c)** Reflection spectra of the off-cavity region as a function of UV irradiation time. UV irradiation gradually decreases the strength of the closed isomer reflectance feature. **(d)** Reaction rate plot of an off-resonance fulgide cavity used to calibrate the UV intensity difference. The linear trend indicates no obvious rate change inside the cavity **(e)** Reaction rate plot of a resonant fulgide cavity. Modeling the photoswitching kinetics reveals accelerated switching in the strong coupling regime.

Spectrally, the two reactions look quite similar, with only the red-shifted photoswitch isomer able to couple to the cavity. Analogously to Hutchison,[17] we here lay down a kinetic model that assumes the species C^*, E^*, and I are in their stationary states, and the rate of excitation of both species is equal. A small difference between the kinetic models for the isomerization of the fulgide and the merocyanine is introduced to account for the fact that there is an intermediate state along the reaction coordinate when going from the closed isomer to the open isomer of the fulgide, but the backwards reaction proceeds in an ultrafast fashion.[23] This kinetic model is shown in **Figure 4**. Note that this kinetic model does not explicitly include the processes from the S_n into S_1 after off-resonant pumping of C. Instead, since these processes are ultrafast, they are incorporated in the rate constants k_2. The kinetic equation for the concentration of the closed isomer $[C]$ is given by Eq 4.

$$\frac{d[C]}{dt} = -k([C] - [C]_\infty) \tag{3}$$

where $k = k_{EX}\left[\left(\frac{k_2}{k_1+k_2}\right)\left(\frac{k_3}{k_3+k_3'}\right) + \left(\frac{k_2'}{k_1'+k_2'}\right)\right]$.

This kinetic equation yields Eq 2 upon integration, which implies that the speed at which the system reaches the PSS (the slope in Figures 3d and 4b) is given by k.

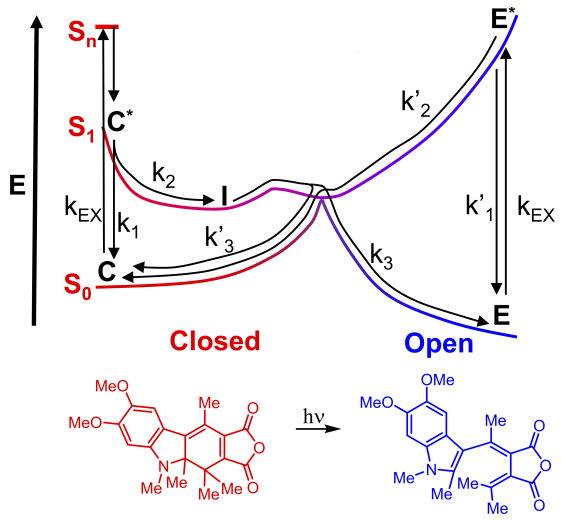

Figure 4. Kinetic model for photoswitching of the fulgide. k_{EX} is the excitation rate. k_1 and k_1' are the sum of radiative and non-radiative decay rates of the closed and open isomers. k_2 and k_2' are the rates from the corresponding excitons into the intermediate state and the ground state of the closed isomer. k_3 and k_3' are the rates from the intermediate state to each of the reactants in the ground state. The shape of the Potential Energy Surface for this reaction is taken from ref.[23]

Inside of the fulgide cavity, the kinetics are not well described by a linear equation due to variation of the Rabi splitting as the reaction proceeds. This non-linearity suggests a time dependence of k due to collective strong coupling. It also suggests that changes in k are due to changes in elementary rate constants involving the closed isomer (k_1, k_2, k_3), which is the only species present in the cavity initially. These changes in rate constants are consistent with the fact that k converges to the off-cavity case at long times when polaritons vanish, and that PSS concentrations in and out of the cavity are identical.

Theoretical models suggest that major polariton-induced modifications of excited-state reactivity occur near the ground state geometry.[24–26] Therefore, here we assume that k_3 remains unchanged and we explain the differences between the on- and off-cavity rates as changes in k_1 or k_2. According to Figure 3e, k increases inside of the fulgide cavity at short times, which can only be explained by an increase in reaction efficiency for the closed isomer, $\left(\frac{k_2}{k_1+k_2}\right)$. This increase is the opposite of what is observed in the SPI/MC experiments, where both we and Hutchison observe a decrease in k under strong coupling.[17] This decrease in k can arise from an increase in the radiative decay k_1 due to cavity leakage of the lower polariton. A similar mechanism for the fulgide, where modified photon density in the cavity leads to a change in radiative decay rate, can be ruled out because the fulgide is non-fluorescent (**Figure S8**). For the fulgide, one may think that the cavity suppresses the dynamics along vibrational modes orthogonal to the reaction coordinate,[24,25] decreasing the non-radiative decay rate, and therefore decreasing k_1. However, this mechanism cannot readily explain why suppression does not occur along the reaction coordinate as well. Therefore, we believe that the cavity serves to increase the rate of fulgide isomerization, k_2.

Although no theoretical model at present can explain the increase of k_2 inside of the fulgide cavity, we propose the following two mechanisms. First, immediately following excitation (timescale of fs), k_2 strongly depends on the ultrafast nonadiabatic dynamics from the bright state of S_n into S_1 before isomerization, which could be modified by off-resonant coupling to the cavity mode. Second, following relaxation to S_1 (timescale of tens of ps, longer than intramolecular energy redistribution and intersystem crossing rates), k_2 depends only on the dynamics in the electronic state S_1 after ultrafast nonadiabatic dynamics from S_n. In one of our most recent theoretical works, we have demonstrated that this second scenario gives rise to molecules in S_1 in the dark-state manifold.[26] Previous works have suggested that reactivity of the dark states is different from that of the molecules outside of the cavity.[27,28] Even if the proposed mechanisms only generate small changes in reactivity (say, the changes are inversely proportional to the number of molecules in the system), small changes might be detectable at macroscopic timescales. In summary, while cavity-induced suppression of merocyanine switching can be explained by enhanced radiative decay rates, enhancement of fulgide switching can currently best be explained by direct modification of excited-state reaction kinetics.

CONCLUSION

We studied the effect of strong light-matter coupling on the kinetics of photoswitching in optical cavities. We recapitulated previously published results in a spiropyran/merocyanine (SPI/MC) system in which strong coupling acts to suppress the photoisomerization between SPI and MC. We reported the first observation of polariton-*enhanced* photochemistry in a photoswitch system, in which the rate of photoisomerzation between two fulgide isomers is increased in the strong coupling regime. While the reproduced SPI/MC results can be explained by modification of radiative decay rates within the cavity, modified switching of the nonfluorescent fulgides can currently only be explained by direct changes to excited state reaction kinetics within the cavity. At present, no theoretical model can explain these changes. The simulation of cavity-modified ultrafast dynamics and chemical reactivity to explain our observations as well as other experimental results in the literature, will be the aim of future work.

ASSOCIATED CONTENT

Supporting Information

Experimental procedures, ^{1}H and ^{13}C NMR spectra, UV-vis and photoluminescence spectra

AUTHOR INFORMATION

Corresponding Author

* jkalow@northwestern.edu, jyuenzhou@ucsd.edu, n-stern@northwestern.edu

Present Addresses

†If an author's address is different than the one given in the affiliation line, this information may be included here.

ACKNOWLEDGMENT

H.Z., P.L., J.B.P.-S., J.Y.-Z., and N.P.S. were supported as part of the Center for Molecular Quantum Transduction (CMQT), an Energy Frontier Research Center funded by the U.S. Department of Energy (DOE), Office of Science, Basic Energy Sciences (BES), under Award

#DE-SC0021314 (molecules integrated in microcavities, polariton theory). C.T.E., W.J.C., E.A.W., and J.A.K. were supported by the Northwestern University Materials Research Science and Engineering Center (MRSEC) (NSF DMR-1720139). C.T.E. acknowledges support from a National Science Foundation Graduate Research Fellowship (grant no. DGE-1842165). This work made use of the IMSERC at Northwestern University, which has received support from the Soft and Hybrid Nanotechnology Experimental (SHyNE) Resource (NSF ECCS-1542205), the State of Illinois, and the International Institute for Nanotechnology (IIN). This work also made use of the MatCI and MLTOF facilities supported by the MRSEC program of the National Science Foundation at the Materials Research Center of Northwestern University.

REFERENCES

(1) Ribeiro, R. F.; Martínez-Martínez, L. A.; Du, M.; Campos-Gonzalez-Angulo, J.; Yuen-Zhou, J. Polariton Chemistry: Controlling Molecular Dynamics with Optical Cavities. *Chem. Sci.* **2018**, *9* (30), 6325–6339. https://doi.org/10.1039/C8SC01043A.

(2) Hertzog, M.; Wang, M.; Mony, J.; Börjesson, K. Strong Light–Matter Interactions: A New Direction within Chemistry. *Chem. Soc. Rev.* **2019**, *48* (3), 937–961. https://doi.org/10.1039/C8CS00193F.

(3) Du, M.; Ribeiro, R. F.; Yuen-Zhou, J. Remote Control of Chemistry in Optical Cavities. *Chem* **2019**, *5* (5), 1167–1181. https://doi.org/10.1016/j.chempr.2019.02.009.

(4) Garcia-Vidal, F. J.; Ciuti, C.; Ebbesen, T. W. Manipulating Matter by Strong Coupling to Vacuum Fields. *Science* **2021**, *373* (6551). https://doi.org/10.1126/science.abd0336.

(5) Ahn, W.; Triana, J.; Recabal, F.; Herrera, F.; Simpkins, B. Modification of Ground State Chemical Reactivity via Light-Matter Coherence in Infrared Cavities. ChemRxiv March 20, 2023. https://doi.org/10.26434/chemrxiv-2022-wb6vs-v2.

(6) Eizner, E.; Martínez-Martínez, L. A.; Yuen-Zhou, J.; Kéna-Cohen, S. Inverting Singlet and Triplet Excited States Using Strong Light-Matter Coupling. *Sci. Adv.* **2019**, *5* (12), eaax4482. https://doi.org/10.1126/sciadv.aax4482.

(7) Liu, B.; Menon, V. M.; Sfeir, M. Y. The Role of Long-Lived Excitons in the Dynamics of Strongly Coupled Molecular Polaritons. *ACS Photonics* **2020**, *7* (8), 2292–2301. https://doi.org/10.1021/acsphotonics.0c00895.

(8) Krainova, N.; Grede, A. J.; Tsokkou, D.; Banerji, N.; Giebink, N. C. Polaron Photoconductivity in the Weak and Strong Light-Matter Coupling Regime. *Phys. Rev. Lett.* **2020**, *124* (17), 177401. https://doi.org/10.1103/PhysRevLett.124.177401.

(9) Polak, D.; Jayaprakash, R.; Lyons, T. P.; Martínez-Martínez, L. Á.; Leventis, A.; Fallon, K. J.; Coulthard, H.; Bossanyi, D. G.; Georgiou, K.; Petty, II, A. J.; Anthony, J.; Bronstein, H.; Yuen-Zhou, J.; Tartakovskii, A. I.; Clark, J.; Musser, A. J. Manipulating Molecules with Strong Coupling: Harvesting Triplet Excitons in Organic Exciton Microcavities. *Chem. Sci.* **2020**, *11* (2), 343–354. https://doi.org/10.1039/C9SC04950A.

(10) Zhong, X.; Chervy, T.; Zhang, L.; Thomas, A.; George, J.; Genet, C.; Hutchison, J. A.; Ebbesen, T. W. Energy Transfer between Spatially Separated Entangled Molecules. *Angew. Chem. Int. Ed.* **2017**, *56* (31), 9034–9038. https://doi.org/10.1002/anie.201703539.

(11) Stranius, K.; Hertzog, M.; Börjesson, K. Selective Manipulation of Electronically Excited States through Strong Light–Matter Interactions. *Nat. Commun.* **2018**, *9* (1), 2273. https://doi.org/10.1038/s41467-018-04736-1.

(12) Zhong, X.; Chervy, T.; Wang, S.; George, J.; Thomas, A.; Hutchison, J. A.; Devaux, E.; Genet, C.; Ebbesen, T. W. Non-Radiative Energy Transfer Mediated by Hybrid Light-Matter States. *Angew. Chem. Int. Ed.* **2016**, *55* (21), 6202–6206. https://doi.org/10.1002/anie.201600428.

(13) Coles, D. M.; Somaschi, N.; Michetti, P.; Clark, C.; Lagoudakis, P. G.; Savvidis, P. G.; Lidzey, D. G. Polariton-Mediated Energy Transfer between Organic Dyes in a Strongly Coupled Optical Microcavity. *Nat. Mater.* **2014**, *13* (7), 712–719. https://doi.org/10.1038/nmat3950.

(14) Marinez-Martinez, L. A.; Du, M.; Ribeiro, R. F.; Kena-Cohen, S.; Yuen-Zhou, J. Polariton-Assisted Singlet Fission in Acene Aggregates. *J. Phys. Chem. Lett.* **2018**, *9* (8), 1951–1957.

(15) Georgiou, K.; Jayaprakash, R.; Othonos, A.; Lidzey, D. Ultralong-Range Polariton-Assisted Energy Transfer in Organic Microcavities. *Angew. Chem. Int. Ed. n/a* (n/a). https://doi.org/10.1002/anie.202105442.

(16) Dovzhenko, D. S.; Lednev, M.; Mochalov, K.; Vaskan, I.; Rakovich, Y.; Karaulov, A.; Nabiev, I. Polariton-Assisted Manipulation of Energy Relaxation Pathways: Donor–Acceptor Role Reversal in a Tuneable Microcavity. *Chem. Sci.* **2021**. https://doi.org/10.1039/D1SC02026A.

(17) Hutchison, J. A.; Schwartz, T.; Genet, C.; Devaux, E.; Ebbesen, T. W. Modifying Chemical Landscapes by Coupling to Vacuum Fields. *Angew. Chem. Int. Ed.* **2012**, *51* (7), 1592–1596. https://doi.org/10.1002/anie.201107033.

(18) Mony, J.; Climent, C.; Petersen, A. U.; Moth-Poulsen, K.; Feist, J.; Börjesson, K. Photoisomerization Efficiency of a Solar Thermal Fuel in the Strong Coupling Regime. *Adv. Funct. Mater. n/a* (n/a), 2010737. https://doi.org/10.1002/adfm.202010737.

(19) Schwartz, T.; Hutchison, J. A.; Genet, C.; Ebbesen, T. W. Reversible Switching of Ultrastrong Light-Molecule Coupling. *Phys. Rev. Lett.* **2011**, *106* (19), 196405. https://doi.org/10.1103/PhysRevLett.106.196405.

(20) Yokoyama, Y. Fulgides for Memories and Switches. *Chem. Rev.* **2000**, *100* (5), 1717–1740. https://doi.org/10.1021/cr980070c.

(21) Yokoyama, Y.; Sagisaka, T.; Mizuno, Y.; Yokoyama, Y. Role of the Methoxy Substituents on the Photochromic Indolylfulgides. Absorption Maximum vs. Molar Absorption Coefficient of the Colored Form. *Chem. Lett.* **1996**, *25* (8), 587–588. https://doi.org/10.1246/cl.1996.587.

(22) Hayashi, S.; Ishigaki, Y.; Fujii, M. Plasmonic Effects on Strong Exciton-Photon Coupling in Metal-Insulator-Metal Microcavities. *Phys. Rev. B* **2012**, *86* (4), 045408. https://doi.org/10.1103/PhysRevB.86.045408.

(23) Tomasello, G.; Bearpark, M. J.; Robb, M. A.; Orlandi, G.; Garavelli, M. Significance of a Zwitterionic State for Fulgide Photochromism: Implications for the Design of Mimics. *Angew. Chem. Int. Ed.* **2010**, *49* (16), 2913–2916. https://doi.org/10.1002/anie.200907250.

(24) Galego, J.; Garcia-Vidal, F. J.; Feist, J. Suppressing Photochemical Reactions with Quantized Light Fields. *Nat. Commun.* **2016**, *7* (1), 13841. https://doi.org/10.1038/ncomms13841.

(25) Herrera, F.; Spano, F. C. Cavity-Controlled Chemistry in Molecular Ensembles. *Phys. Rev. Lett.* **2016**, *116* (23), 238301. https://doi.org/10.1103/PhysRevLett.116.238301.

(26) Pérez-Sánchez, J. B.; Koner, A.; Stern, N. P.; Yuen-Zhou, J. Simulating Molecular Polaritons in the Collective Regime Using Few-Molecule Models. *Proc. Natl. Acad. Sci.* **2023**, *120* (15), e2219223120. https://doi.org/10.1073/pnas.2219223120.

(27) Wellnitz, D.; Pupillo, G.; Schachenmayer, J. Disorder Enhanced Vibrational Entanglement and Dynamics in Polaritonic Chemistry. *Commun. Phys.* **2022**, *5* (1), 1–11. https://doi.org/10.1038/s42005-022-00892-5.

(28) Du, M.; Yuen-Zhou, J. Catalysis by Dark States in Vibropolaritonic Chemistry. *Phys. Rev. Lett.* **2022**, *128* (9), 096001. https://doi.org/10.1103/PhysRevLett.128.096001.

TOC graphic:

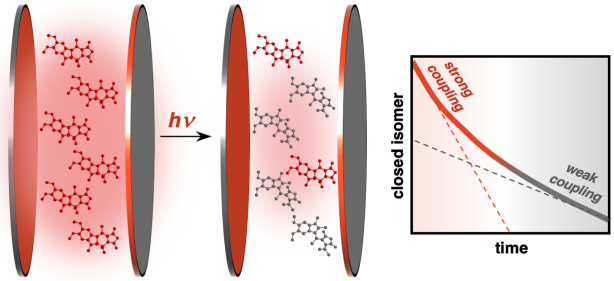

Supporting Information

Control of photoswitching kinetics with strong light-matter coupling in a cavity

Hongfei Zeng,[1] Pufan Liu,[1] Christopher T. Eckdahl,[2] Juan B. Pérez-Sánchez,[3] Woo Je Chang,[2,4] Emily A. Weiss,[2,4] Julia A. Kalow,*[2] Joel Yuen-Zhou,*[3] Nathaniel P. Stern*[1]

[1]Department of Physics and Astronomy, Northwestern University, Evanston, IL 60208, United States
[2]Department of Chemistry, Northwestern University, Evanston, IL 60208, United States
[3]Department of Chemistry and Biochemistry, University of California–San Diego, La Jolla, CA 92093, United States
[4]Department of Materials Science and Engineering, Northwestern University, Evanston, IL 60208, United States

Table of Contents

General Information

General procedures. Unless otherwise noted, reactions were performed under N_2 atmosphere in oven-dried (150 ºC) glassware. Reaction progress was monitored by thin layer chromatography (EMD 250 μm silica gel 60-F254 plates) or by liquid chromatography-mass spectrometry using a Agilent 6120 Quadrupole LC/MS. Automated column chromatography was performed using SiliCycle SiliaFlash F60 (40-63 μm, 60 Å) in SNAP cartridges on a Biotage Isolera One. Organic solvents were removed in vacuo using a rotary evaporator (Büchi Rotovapor R-100, ~20–200 torr) and residual solvent was removed under high vacuum (<0.1 torr).

Materials. Commercial reagents were purchased from Sigma-Aldrich, Acros, Alfa Aesar, TCI, or Oakwood and used as received. Disiopropylamine was distilled from calcium hydride prior to use. THF and dichloromethane were purified and dried using a solvent-purification system that contained activated alumina then degassed with N_2 sparging prior to use.

Instrumentation. Proton nuclear magnetic resonance (^{1}H NMR) spectra and carbon nuclear magnetic resonance (^{13}C NMR) spectra were recorded on Bruker AVANCE-500 spectrometers at 500 MHz and 125 MHz, and referenced to the solvent residual peaks. NMR data are represented as follows: chemical shift (δ ppm), multiplicity (s = singlet, d = doublet, t = triplet, q = quartet, m =

multiplet), coupling constant in Hertz (Hz), integration. UV-vis spectra were collected on a Cary 5000 UV-vis-NIR spectrophotometer with an Hg lamp; cuvettes were 10-mm path length quartz cells (Starna 23-Q-10).

Synthesis

We synthesized the indolyl fulgide studied in this work following a previously published procedure.[1] However, since synthetic and spectral details are lacking in the literature report, we will provide detailed account of our synthesis.

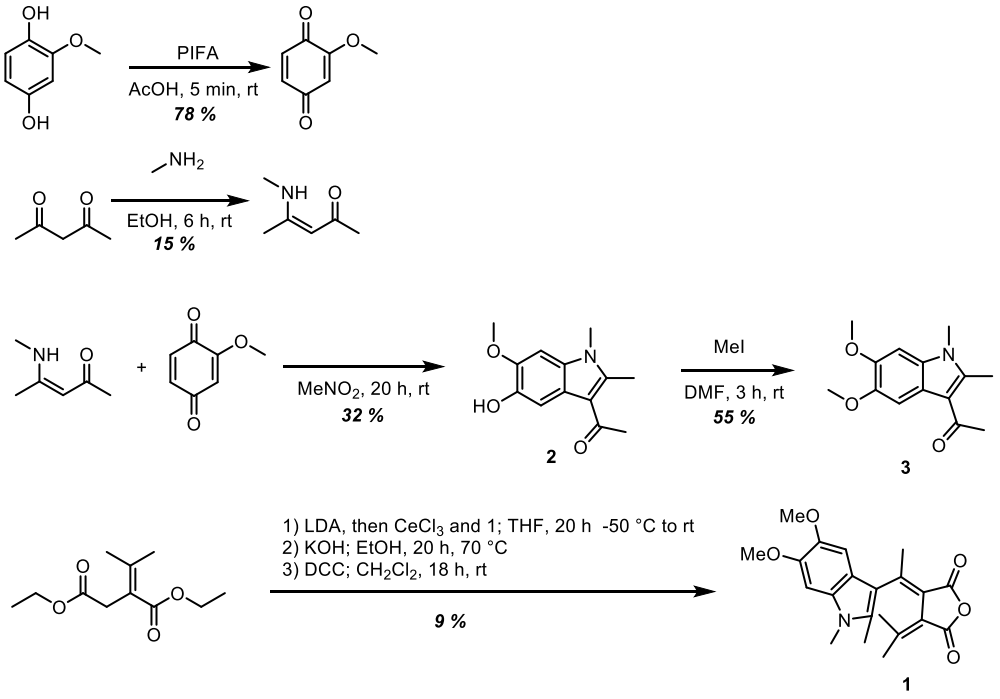

Scheme 1. Synthesis of the indolyl fulgide studied in this work.

2-methoxycyclohexa-2,5-diene-1,4-dione was synthesized following a literature procedure.[2] 10.0 g (71.36 mmol) of 2-methoxybenzene-1,4-diol was dissolved in 500 mL of acetic acid in an open beaker with a stir bar. Phenyl-I3-iodanediyl bis(2,2,2-trifluoroacetate) (61.37 g, 142.7 mmol) was added all at once, causing an immediate color change to brown then quickly yellow. After stirring at room temperature for 3 minutes, 200 mL water was added, causing a precipitate to form. The mixture was

neutralized with sat. $NaHCO_3$, then was extracted with 3 X 100 mL of dichloromethane. The combined organic layers were dried over Na_2SO_4, then the solvent removed *in vacuo*. The crude product was purified by silica chromatography with a 2:1 hexane/ethyl acetate mobile phase. A pure yellow solid was isolated following solvent removal (9.86 g, 78 % yield). ^{1}H NMR matched the literature report.

(Z)-4-(methylamino)pent-3-en-2-one was synthesized following a literature procedure.[3] Methylamine (50 mL of a 40 wt% solution in ethanol, 0.1 mol) was added to 51 mL (0.50 mol) of pentane-2,4,-dione and the mixture was stirred for 2 h at room temperature. The mixture was then suspended in 60 mL diethyl ether and 60 mL water. The organic layer was separated, then the aqueous layer was extracted with 3 x 20 mL of diethyl ether. The combined organic layers were washed with brine and dried over $MgSO_4$. Removal of the solvent *in vacuo* provided a yellow oil that crystallized upon standing. The product was purified by recrystallization from 20 mL of diethyl ether, providing colorless needle-like crystals (9.15 g, 15 % yield). ^{1}H NMR matched the literature report.

1-(5-hydroxy-6-methoxy-1,2-dimethyl-1H-indol-3-yl)ethan-1-one (2) was synthesized based on a literature procedure for a related compound.[3] 2-methoxycyclohexa-2,5-diene-1,4-dione (7.68 g, 55.6 mmol) was dissolved in 10 mL of dry nitromethane in a flame-dried Schlenk flask with a stir bar. In a separate flame-dried flask, (Z)-4-(methylamino)pent-3-en-2-one (6.29 g, 55.6 mmol) was dissolved in 40 mL of dry nitromethane. The yellow enaminone solution was added to the orange dione slurry all at once, immediately producing a dark scarlet / brown mixture. The reaction was stirred under N_2 at room temperature for 19 h, after which time the slurry had become white. The white solid was filtered off and washed with nitromethane then diethyl ether. The product was isolated by repeated trituration in methanol (note that heading leads to oxidation to a deeply blue indigo, thus recrystallization was avoided). The colorless solid was dried *in vacuo* to yield the pure product (4.18 g, 32 % yield). ^{1}H NMR

(500 MHz, DMSO) δ 8.56 (s, 1H), 7.40 (s, 1H), 7.07 (s, 1H), 3.83 (s, 3H), 3.67 (s, 3H), 2.65 (s, 3H), 2.46 (s, 3H). ^{13}C NMR (126 MHz, DMSO) δ 192.52, 146.41, 144.02, 142.07, 130.23, 119.22, 112.90, 106.14, 93.53, 55.99, 31.62, 29.67, 11.57.

1-(5,6-dimethoxy-1,2-dimethyl-1H-indol-3-yl)ethan-1-one (3) was synthesized based on a literature procedure for a related compound.[3] 1-(5-hydroxy-6-methoxy-1,2-dimethyl-1H-indol-3-yl)ethan-1-one (4.18 g, 17.9 mmol) was dissolved in 120 mL of dry DMF in a flame-dried Schlenk flask with a stir bar. The mixture was cooled in an ice bath. Sodium hydride (788 mg of a 60 wt% mixture with mineral oil, 19.7 mmol) was added all at once, producing an orange color. The mixture was stirred under N_2 at 0 °C for 1 h. Then, methyl iodide (1.23 mL, 19.7 mmol) was added dropwise over 5 min. The reaction was removed from cooling and continued stirring. The reaction developed a dark purple color and gradually homogenized. After 3 h, the reaction was quenched with 200 mL of 1 M HCl, then extracted with 3 X 150 mL of ethyl acetate. The combined organic layers were rinsed with brine then dried over Na_2SO_4. After solvent removal, the product was purified by column chromatography (4:1 toluene/acetone mobile phase), yielding a slightly pink solid (2.42 g, 55 % yield) after solvent removal *in vacuo*. ^{1}H NMR (500 MHz, DMSO) δ 7.51 (s, 1H), 7.11 (s, 1H), 3.81 (s, 3H), 3.77 (s, 3H), 3.68 (s, 3H), 2.65 (s, 3H), 2.50 (s, 3H). ^{13}C NMR (126 MHz, DMSO) δ 192.77, 146.43, 145.87, 142.65, 130.73, 118.68, 113.40, 103.51, 94.41, 55.90, 31.16, 29.78, 12.62.

(Z)-3-(1-(5,6-dimethoxy-1,2-dimethyl-1H-indol-3-yl)ethylidene)-4-(propan-2-ylidene)dihydrofuran-2,5-dione (1) was synthesized based on a literature procedure for a related compound.[3] Cerium (III) chloride heptahydrate (3.65 g, 9.79 mmol) was dried under vacuum at 140 °C with stirring. The $CeCl_3$ was put under N_2 and cooled to RT. Then, 700 μL of dried, degassed THF was added and the suspension was stirred under N_2 overnight. In a separate flask, diisopropylamine (1.93 mL, 13.7 mmol) was dissolved in 30 mL of dry THF and cooled to -50 °C in a 50 %

methanol/water dry ice bath. Butyllithium (5.09 mL of a 2.5 M hexanes solution) was added to the amine to form a slightly yellow solution of lithium diisopropyl amide (LDA). Diethyl 2-(propan-2-ylidene)succinate (2.31 g, 10.8 mmol) was dissolved in 30 mL of dry THF and cooled to -50 °C. The succinate solution was transferred to the LDA solution over about 5 min *via* cannula. The combined solution was stirred at -50 °C for 30 min to form the lithium enolate.

Separately, 1-(5,6-dimethoxy-1,2-dimethyl-1H-indol-3-yl)ethan-1-one (2.42 g, 9.79 mmol) was dissolved in 15 mL of dry THF in a Schlenk flask with a stir bar and cooled to 0 °C in an ice bath. The $CeCl_3$ was quickly cannula transferred to the indole solution, then the combined mixture was cooled to -50°C. The lithium enolate solution from above was then slowly cannula transferred to the indole, $CeCl_3$ slurry over 5 min. The reaction flask was covered with aluminum foil to exclude light, then left stirring under N_2 as the cooling bath gradually warmed to room temperature overnight. After 19 h, 50 mL of saturated ammonium chloride was added, causing the brown slurry to turn orange and produce additional precipitate. The mixture was filtered through celite, then 50 mL of 1 M HCl was added to the filtrate. The mixture was extracted with 3 X 100 mL ethyl acetate and the combined organic layers were washed with brine and dried over Na_2SO_4. The solvent was removed in *vacuo*, then the crude material was dissolved in 1:1 cyclohexane/ethyl acetate and passed through a silica plug. Solvent removal produced an orange oil.

The oil was dissolved in 60 mL of ethanol and 5 mL of saturated potassium hydroxide was added. The reaction was stirred under N_2 at 70 °C for 20 h, gradually darkening from yellow to brown. After cooling to room temperature, the reaction was poured onto ice then extracted with 100 mL diethyl ether and 100 mL hexanes. The aqueous layer was collected, acidified with HCl, and extracted with 3 X 100 mL ethyl acetate. The combined organic layers were washed with brine and dried over Na_2SO_4. Removal of solvent *in vacuo* provided a brown wax.

The brown wax was dissolved in 50 mL of dry dichloromethane in a dry Schlenk flask. Dicyclohexylmethanediimine (4.04 g, 19.6 mmol) was added and the flask was wrapped in aluminum foil to exclude light. The reaction was stirred at room temperature under N_2 for 18 h, then passed through a silica plug, yielding a yellow solution. Solvent was removed *in vacuo*, then the product was purified by column chromatography (linear gradient of ethyl acetate/hexanes). After solvent removal, the yellow powder was further purified by recrystallization from 30 mL of isopropyl alcohol, yielding a yellow solid (341 mg, 9 % yield). Based on switching experiments, the isolated product was 94 % *Z* isomer and 6 % *E* isomer. ^{1}H NMR (400 MHz, $CDCl_3$) δ 6.75 (s, 1H), 6.69 (s, 1H), 3.96 (s, 3H), 3.87 (s, 3H), 3.65 (s, 3H), 2.79 (s, 3H), 2.25 (s, 3H), 2.19 (d, J = 2.8 Hz, 3H), 0.94 (s, 3H).

Cavity fabrication

The fulgide cavity sample was prepared as follows. The bottom Ag layer (80 nm thick) was deposited onto a silicon substrate by a thermal evaporator (Kurt Lesker Nano38). The PVA was spincoated (1.5% by weight aqueous solution at 4500 rpm) onto the sample. Then the PMMA containing the fulgide molecules was spincoated (1.5% by weight PMMA and 2.5% by weight fulgide in anisole at 4500 rpm) before adding the second PVA layer. The top Ag film (60 nm thick) was evaporated onto the partially covered sample to create an off-cavity region. For off-resonance cavity the PMMA containing fulgide and the PVA were spincoated at 3000 rpm. The thicknesses of the PVA and PMMA layers are 30 nm and 120 nm, respectively.

The SPI cavity was fabricated following a similar procedure except that different solution and spincoating parameters were used. The PVA (0.8% by weight aqueous solution) was spincoated at 4800 rpm, while the PMMA containing SPI (1.3% by weight PMMA and 2.1% by weight SPI in anisole) was spincoated at 2800 rpm. The thicknesses of the PVA and PMMA layers are 15 nm and 110 nm, respectively.

Photoluminescence (PL) measurement

The fulgide and MC samples for PL measurement were prepared by spincoating their respective solutions onto a 285 nm SiO2/Si substrate. The samples were excited by a He-Cd laser (Kimmon IK Series) at 325 nm. The PL signal was separated from the excitation beam with a 409 nm dichroic mirror and 450 nm long pass filter. The filtered signal was sent to a spectrometer of 303 mm focal length (Andor Shamrock 303i) equipped with a thermoelectric cooled camera (Oxford Instruments DU420A-BEX2-DD). PL spectrum of closed fulgide and MC was measured (Figure S8).

Reflectance measurement

The setup for reflectance measurement is shown in Figure S9. An achromatic lens of 50 mm focal length was used to focus the collimated white light source (Thorlabs SLS 201) onto the sample and collimate the reflected signal. The same spectrometer as in the PL measurement was used to record the reflectance spectrum. The sample was placed in a vacuum chamber under pressure < 0.1 Pa to avoid photooxidation during laser irradiation. The whole setup except the sample stage was mounted on a motorized x-y translation stage to allow for measuring different locations on the sample.

Data analysis

The reflectance spectrum is simulated by transfer matrix method, which uses a transfer matrix to find the relationship between forward and backward electromagnetic waves and solve the reflectance spectrum. The cavity structure is treated as a multilayered structure with various complex refractive

indices and thicknesses. A Lorentz oscillator model of the refractive index is used to account for the polymer matrix including molecules:

$$\tilde{n} = \sqrt{\varepsilon_b + \frac{f\omega_0^2}{\omega_0^2 - \omega^2 - i\gamma\omega}}$$

Here $\tilde{n}$ is the complex refractive index of the polymer matrix with molecules, ε_b is the background permittivity without molecules, ω_0 is the closed isomer exciton energy, γ is the exciton decay rate, and f is the oscillator strength, which is proportional to the closed isomer concentration. Note that the broad feature in the molecule absorption is an effect of additional vibrational modes in addition to the electronic transition as well as inhomogeneous broadening. In the Lorentz model, this is approximated as a single transition with a damping rate to account for the overall molecule linewidth, which captures the main feature. At each irradiation time, the oscillator strength is obtained from a fit to the reflection spectrum, and thus the closed isomer concentration as a function of irradiation time could be extracted for reaction kinematics analysis.

NMR spectra

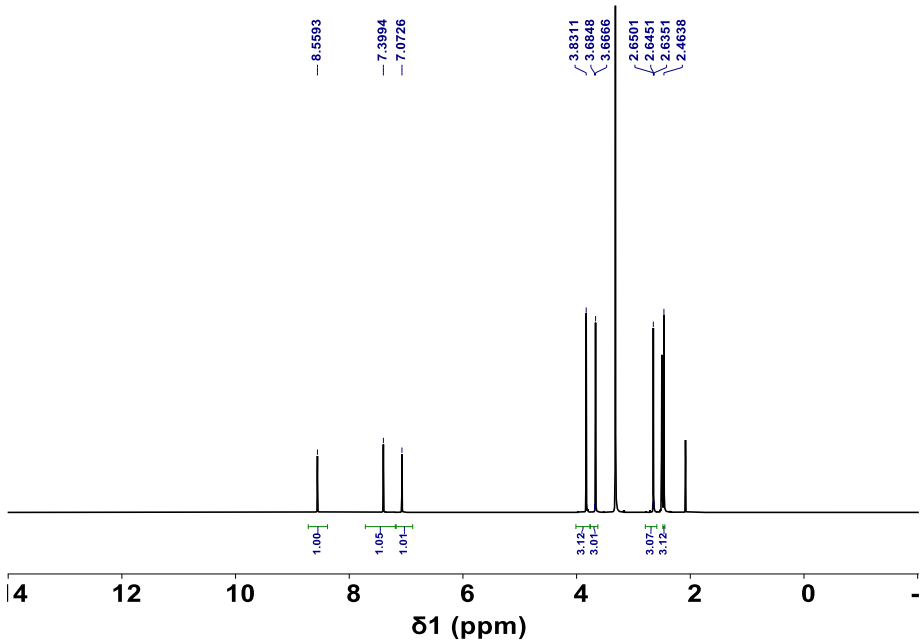

Figure S1. ^{1}H NMR (500 MHz) of **2** in DMSO-*d*$_6$.

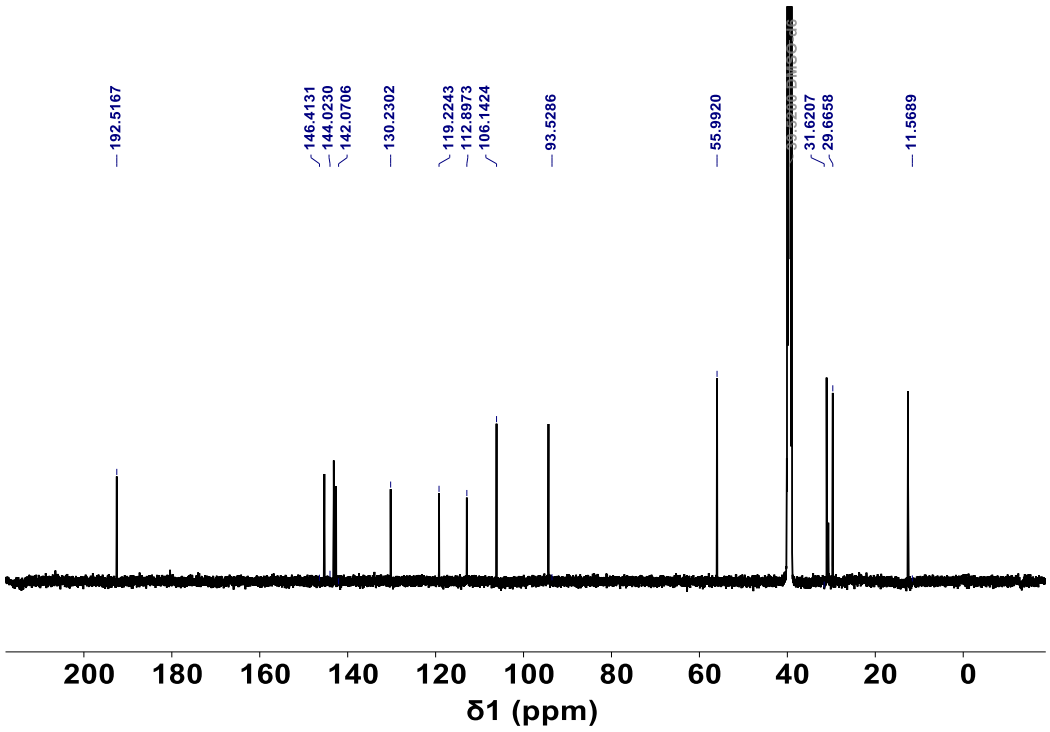

Figure S2. ^{13}C{^{1}H} NMR (126 MHz) of **2** in DMSO-*d*$_6$.

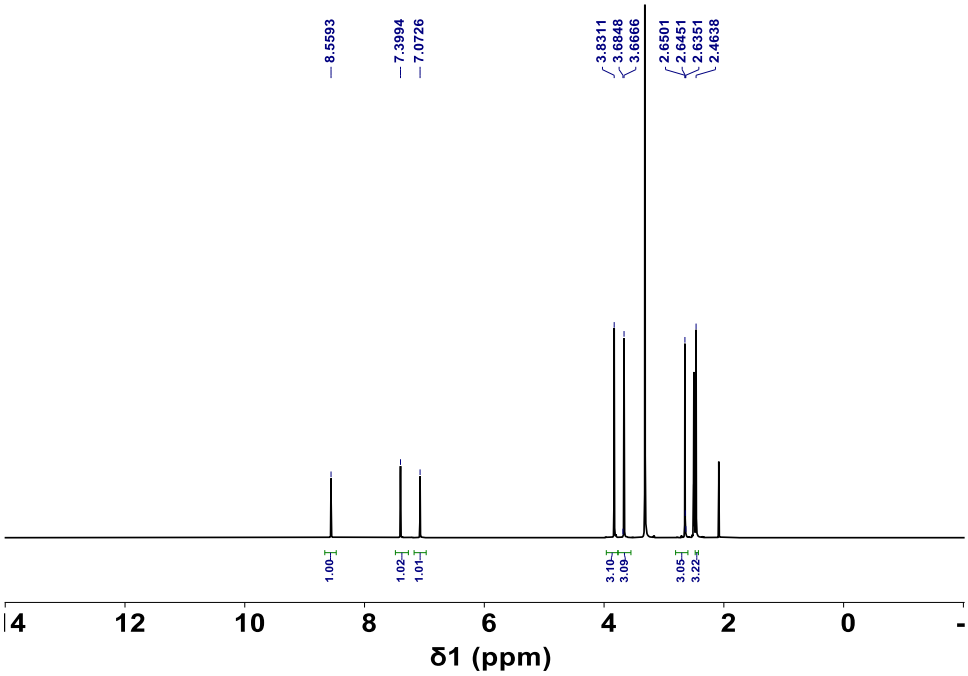

Figure S3. ^{1}H NMR (500 MHz) of **3** in DMSO-*d*$_6$.

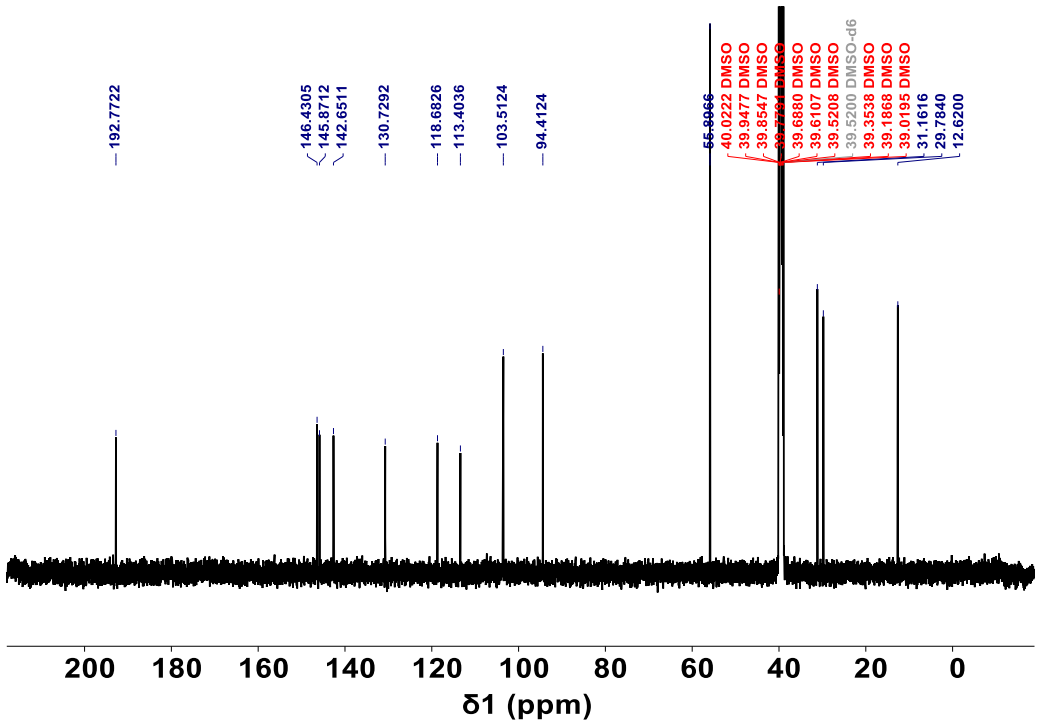

Figure S4. ^{13}C{^{1}H} NMR (126 MHz) of **3** in DMSO-*d*$_6$.

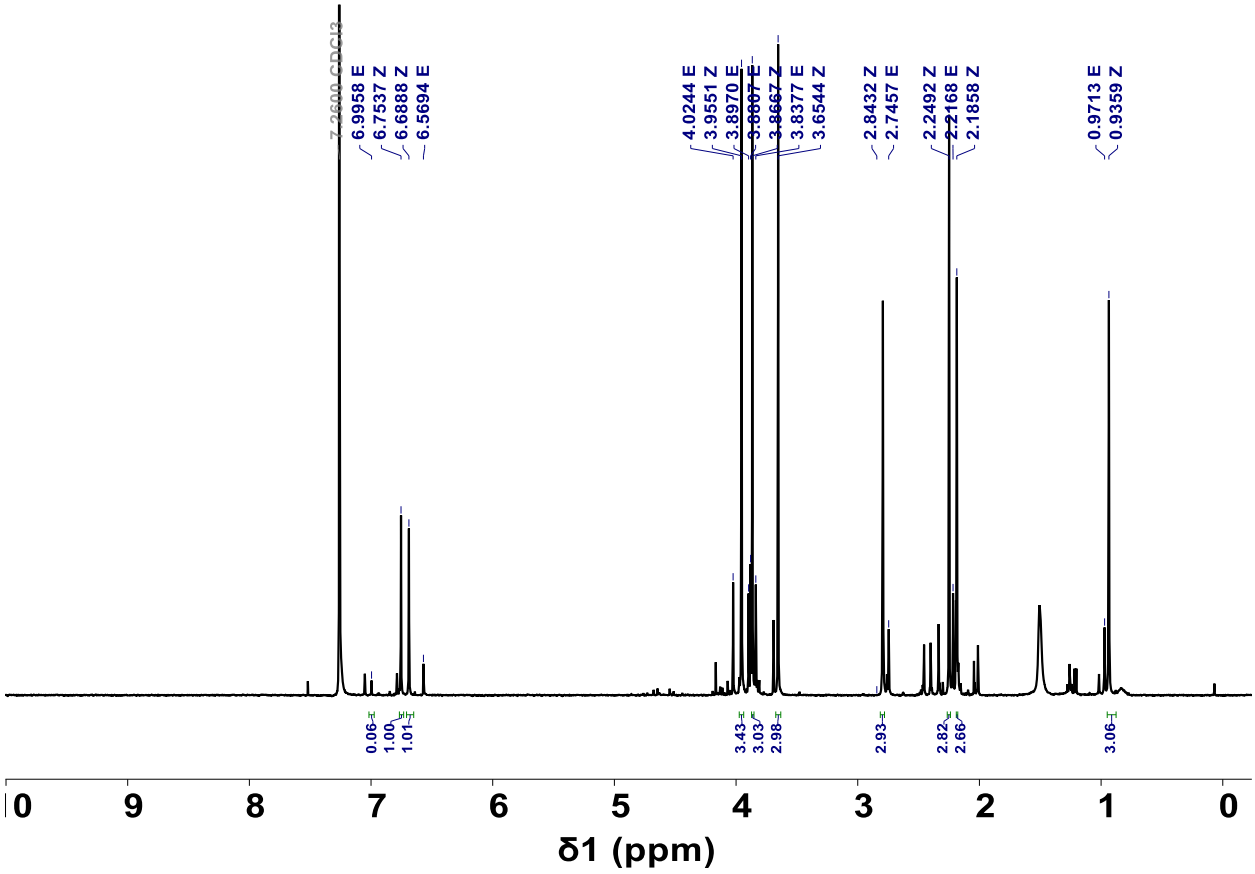

Figure S5. ^{1}H NMR (500 MHz) of **1** in $CDCl_3$. the major product is the *Z* isomer, with ~6 % *E* isomer. "E" and "Z" designations given above peak positions. Integrations are shown for the major product and one isolated peak for the minor product.

UV-Vis and photoluminescence spectra

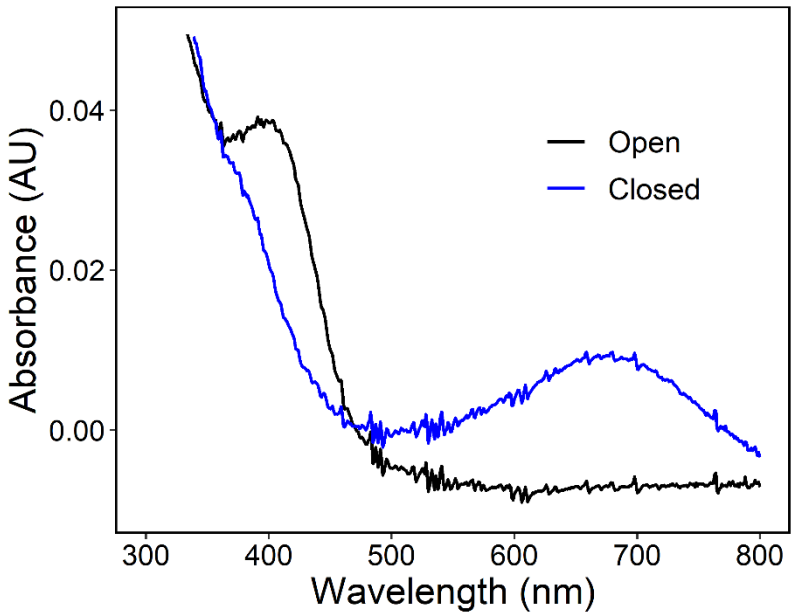

Figure S6. UV-Vis spectrum of the Open and Closed fulgide in a dropcast PMMA film.

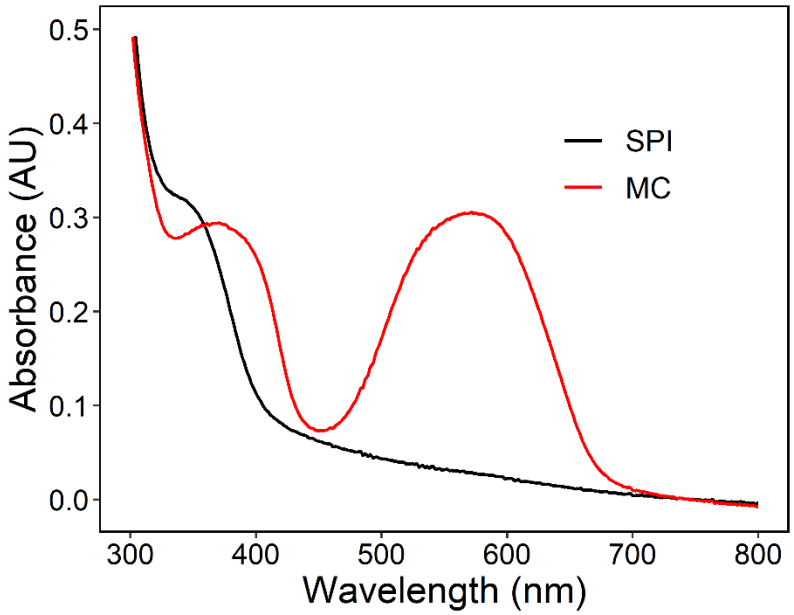

Figure S7. UV-Vis spectrum of SPI and MC in a dropcast PMMA film.

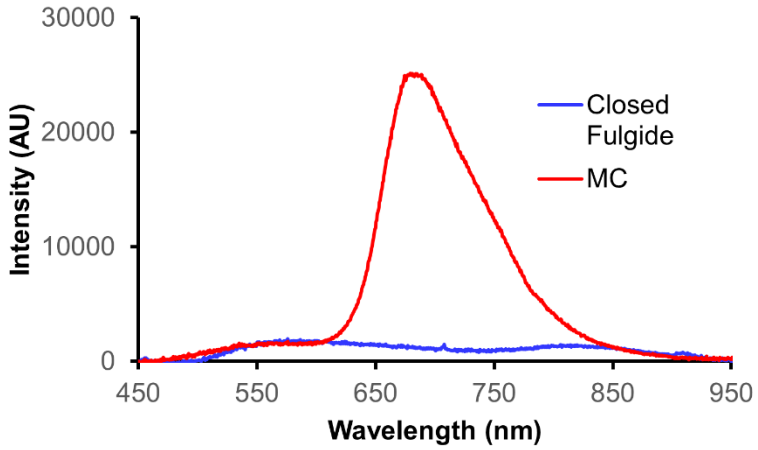

Figure S8. PL spectrum of closed fulgide and MC photoswitches in spincoated PMMA films. The MC is strongly fluorescent while the fulgide is not fluorescent.

Reflectance measurement schematic

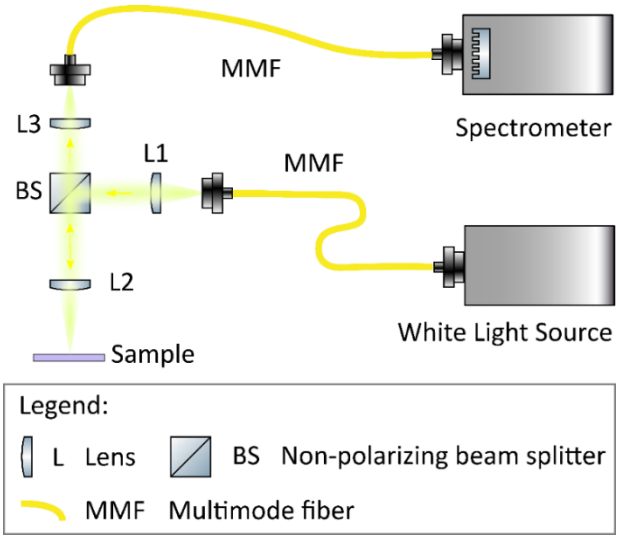

Figure S9. Schematic of setup for reflectance measurement.

Off-resonance sample at all angles for control measurement

In Figure 3d, we measured the photoisomerization of a cavity sample resonant at 830 nm as the control measurement. A cavity mode at 830 nm is far off-resonant from the molecule absorption,

but due to the cavity dispersion at none-zero angles the cavity mode is closer to the molecule absorption. To rule out possible effect of strong coupling at none-zero angles, we also repeated the measurement with another cavity sample resonant at 500 nm at normal incidence, as shown in Figure S10. Similar to Figure 3d, the plots in Figure S10 are also linear in both on-cavity and off-cavity regions, confirming the control measurements are valid.

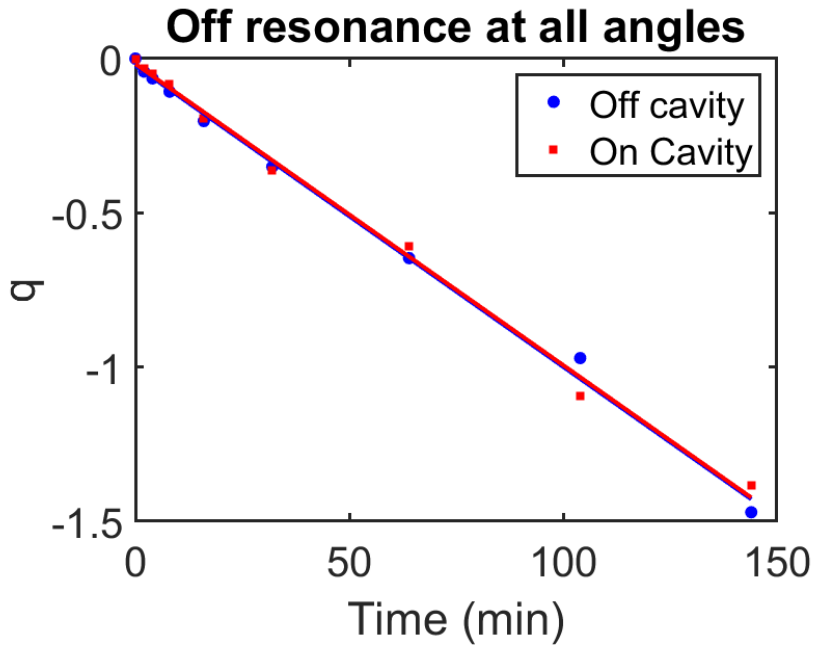

Figure S10. Reaction rate plot of a control fulgide cavity that is off-resonanance at all angles.

Reproduction of previous SPI/MC results

The SPI molecules are commercially available and were dispersed in PMMA inside a cavity with fundamental mode near the MC absorption at 560 nm. The SPI/MC cavity exhibited spectra similar to those already reported by Ebbesen and coworkers.[4] As described in their study, we measured the switching kinetics by starting with a full population of uncoupled SP isomer, then irradiating with 325 nm UV light to trigger isomerization. We analyzed the reflectance spectra as a function of time in the same way as for the fulgide and plot the same quantity $q(t)$ vs. t, this time with the concentration of

MC (**Figure S11**). Because this system ends in the strongly coupled regime, the final concentration is different in the on-cavity and off-cavity regions, as noted above. This difference necessitated different $C(\infty)$ for the "on cavity" and "off cavity" data. Both regions begin with similar kinetics, but the slope magnitude decreases as the "on-cavity" region enters the strong coupling regime. This change indicates that the system is approaching the PSS more slowly once it enters the strong coupling regime, consistent with Ebbesen's previous work.[4]

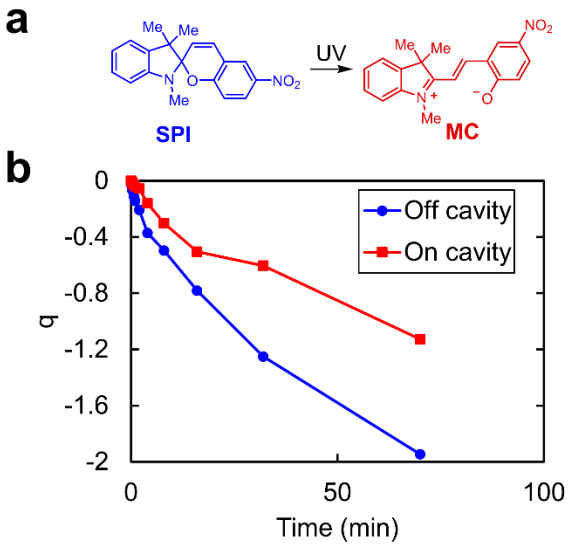

Figure S11. (a) Photoswitching of SP to MC upon UV irradiation. (b) Reaction rate plot of a resonant SP cavity. Modeling of photoswitching kinetics reveals that the molecules in the on-cavity region switch more quickly while in the strong coupling regime, and that a higher amount of MC is present at the PSS.

Works cited

(1) Yokoyama, Y.; Sagisaka, T.; Mizuno, Y.; Yokoyama, Y. Role of the Methoxy Substituents on the Photochromic Indolyfulgides. Absorption Maximum vs. Molar Absorption Coefficient of the Colored Form. *Chem. Lett.* **1996**, *25*, 587–588.

(2) Varlet, T.; Gelis, C.; Retailleau, P.; Bernadat, G.; Neuville, L.; Masson, G. Enantioselective Redox-Divergent Chiral Phosphoric Acid Catalyzed Quinone Diels–Alder Reactions. *Angew. Chem. Int. Ed.* **2020**, *59* (22), 8491–8496. https://doi.org/10.1002/anie.202000838.

(3) Strübe, F.; Rath, S.; Mattay, J. Functionalized Fulgides and Fluorophore-Photoswitch Conjugates. *Eur. J. Org. Chem.* **2011**, *2011* (24), 4645–4653. https://doi.org/10.1002/ejoc.201100228.
(4) Hutchison, J. A.; Schwartz, T.; Genet, C.; Devaux, E.; Ebbesen, T. W. Modifying Chemical Landscapes by Coupling to Vacuum Fields. *Angew. Chem. Int. Ed.* **2012**, *51*, 1592–1596.